


HIF2 α -induced upregulation of *RNASET2* promotes triglyceride synthesis and enhances cell migration in clear cell renal cell carcinoma

Yanmei Quan¹, Jun Dai², Sian Zhou³, Lingyi Zhao³, Lixing Jin³, Yijing Long³, Siwei Liu³, Yanqin Hu¹, Yue Liu¹, Juping Zhao² and Zhide Ding¹ 

¹ Department of Histology, Embryology, Genetics and Developmental Biology, Shanghai Key Laboratory for Reproductive Medicine, Shanghai Jiao Tong University School of Medicine, China

² Department of Urology, Ruijin Hospital, Shanghai Jiao Tong University School of Medicine, China

³ Department of Clinical Medicine, Shanghai Jiao Tong University School of Medicine, China

Keywords

cancer stages; clear cell renal cell carcinoma (ccRCC); HIF2 α ; *RNASET2*; triglycerides synthesis

Correspondence

Y. Liu and Z. Ding, Department of Histology, Embryology, Genetics and Developmental Biology, Shanghai Key Laboratory for Reproductive Medicine, Shanghai Jiao Tong University School of Medicine, Shanghai 200025, China

E-mail: liuyue@shsmu.edu.cn (YL);

zding@shsmu.edu.cn (ZD)

J. Zhao, Department of Urology, Ruijin Hospital, Shanghai Jiao Tong University School of Medicine, Shanghai 200025, China

E-mail: zjp11317@rjh.com.cn

(Received 30 August 2022, revised 6 January 2023, accepted 1 February 2023)

doi:10.1002/2211-5463.13570

Clear cell renal cell carcinoma (ccRCC), the most common malignant subtype of renal cell carcinoma, is characterized by the accumulation of lipid droplets in the cytoplasm. *RNASET2* is a protein coding gene with a low expression level in ovarian cancers, but it is overexpressed in poorly differentiated neuroendocrine carcinomas. There is a correlation between *RNASET2* upregulation and triglyceride expression levels in human serum but it is unknown whether such an association is a factor contributing to lipid accumulation in ccRCC. Herein, we show that *RNASET2* expression levels in ccRCC tissues and cell lines are significantly higher than those in both normal adjacent tissues and renal tubular epithelial cells. Furthermore, its upregulation is associated with increases in ccRCC malignancy and declines in patient survival. We also show that an association exists between increases in both cytoplasmic lipid accumulation and HIF-2 α transcription factor upregulation, and increases in both *RNASET2* and triglyceride expression levels in ccRCC tissues. In addition, DGAT1 and DGAT2, two key enzymes involved in triglyceride synthesis, are highly expressed in ccRCC tissues. By contrast, *RNASET2* knockdown inhibited their expression levels and lowered lipid droplet accumulation, as well as suppressing *in vitro* cell proliferation, cell invasion, and migration. In conclusion, our data suggest HIF2 α upregulates *RNASET2* transcription in ccRCC cells, which promotes both the synthesis of triglycerides and ccRCC migration. As such, *RNASET2* may have the potential as a biomarker or target for the diagnosis and treatment of ccRCC.

According to the Global Cancer Observatory in 2020, the incidence of kidney cancer in males ranks tenth among all cancers in the world. Renal cell carcinoma (RCC) is the most malignant type of kidney cancer

and its incidence is recently increasing worldwide [1]. Four main subtypes of RCC are identifiable based on their histopathological classification. They include clear cell renal carcinoma (ccRCC), chromophobe cell

Abbreviations

ANT, adjacent normal tissue; CCLE, Cancer Cell Line Encyclopedia; ccRCC, clear cell renal cell carcinoma; chRCC, chromophobe cell renal carcinoma; ChIP, chromatin immunoprecipitation; DFS, disease-free survival; DGAT, diacylglycerol O-acyltransferase; GEPIA, gene expression profiling interactive analysis; H&E staining, hematoxylin–eosin; IHC, staining and immunohistochemistry; KEGG, Kyoto Encyclopedia of Genes and Genomes; pRCC, papillary renal cell carcinoma; *RNASET2*, RNase T2; RTCA, real-time cell analysis; TCGA, The Cancer Genome Atlas; TEM, transmission electron microscopy; TG, triglyceride.

renal carcinoma (chRCC), and papillary renal cell carcinoma (pRCC), and collect duct carcinoma. ccRCC is the most common subtype of RCC, which accounts for more than 70% of the total cases, usually accompanying a high rate of metastasis and recurrence [1,2]. Pathological analyses show that ccRCC arises from the epithelial cells lining the lumen of the proximal convoluted tubules in the kidney. Increases in the hematoxylin–eosin (H&E) staining are attributable to rises in cytoplasmic lipid and glycogen content, which caused the cytoplasm to become transparent [3]. Notably, although ccRCC presents a variety of symptoms in its early stages, it often has an asymptomatic clinical manifestation [3,4]. Its clinical diagnosis is hindered by the lack of specific biomarkers, which accounts for its poor prognosis [5]. Therefore, there is an urgent need to identify novel-targeted biomarkers that will enable earlier diagnosis and treatment of ccRCC.

RNASET2 is a single-copy gene located at chromosome 6q27, a region related to cell malignancy and chromosomal rearrangement [6]. It is a secreted protein that is the only member of the Rh/T2/S glycoprotein family expressed in humans. It is present in the cytoplasm outside the perinuclear region, where it colocalizes with endoplasmic reticulum markers and cis/trans-Golgi [7,8]. *RNASET2* has diverse functions, including scavenging ribonucleic acid, degradation of self-RNA, modulating host immune responses, etc. [7–10]. The adipose coexpression networks reveal a correlation between the expression of *RNASET2* in adipocytes and the content of triglycerides in humans [11]. Remarkably, *RNASET2* exerts its ‘antitumor function’ independently of its ribonuclease activity [12]. Several studies documented that *RNASET2* plays a vital role as a tumor suppressor gene in the progression of ovarian tumors and melanomas. However, a recent study showed that *RNASET2* was downregulated in the early stage of gastric adenocarcinoma compared with adjacent noncancerous or normal gastric mucosa tissues, but the knock-down or knockout of *RNASET2* did not significantly promote gastric adenocarcinoma cell growth [13]. Meanwhile, Uccella *et al.* [14] reported that the *RNASET2* protein was significantly highly expressed in poorly differentiated neuroendocrine neoplasms of the lung compared with that in well-differentiated tissues. It suggested that *RNASET2* may instead have different biological effects that are either tumor type-dependent or related to their stage of progression. Besides, the role of *RNASET2* in disrupting lipid metabolism warranted clarification in ccRCC.

In the current study, we show that there are stage-dependent variations in the *RNASET2* expression level relative to their invariance in normal kidney tissue.

This difference prompted us to clarify if: (a) an association exists among *RNASET2* expression levels and ccRCC oncogenesis; (b) dysfunctional lipid metabolism is an underlying mechanism of this pathological condition.

Results

Selective *RNASET2* upregulation in clear cell renal cell carcinoma

Although several studies reported that *RNASET2* is a tumor suppressor gene in ovarian cancer and melanoma [12,15–17], *RNASET2* is overexpressed in poorly differentiated rather than in well-differentiated neuroendocrine neoplasms of the lung [14]. This disconnect prompted us to speculate that *RNASET2* may have diverse expression levels and functions in different tumors. The Broad Institute controls a cancer research project entitled the Cancer Cell Line Encyclopedia (CCLE), which originally focused on characterizing DNA copy numbers, DNA mutations, gene expression, and microRNA profiling, as well as assessing DNA methylation status, across nearly 1000 cell lines from over 30 kinds of cancerous tissues. These studies were appended with metabolite profiling in 2019 [18]. CCLE reveals that the expression of *RNASET2* is significantly higher in kidney cancer than that in other cancers (Fig. 1A). GEPIA2 (Gene Expression Profiling Interactive Analysis 2) developed from GEPIA has been a valuable resource for gene expression analysis based on tumor and normal samples from the TCGA (The Cancer Genome Atlas) and GTEx (Genotype-Tissue Expression) databases [19]. Since ccRCC is the main type of tumor in kidney malignancy, we analyzed using TCGA datasets at GEPIA2 and found that *RNASET2* gene expression was significantly higher in ccRCC tissues compared with that in other cancers (Fig. 1B). Moreover, the expression of *RNASET2* mRNA increased significantly in the advanced stages of ccRCC (Fig. 1C).

We then assessed the survival duration of patients with different *RNASET2* expression levels using TCGA datasets at GEPIA2. Overall survival analysis showed that ccRCC patients with high *RNASET2* expression levels had survival times that were significantly shorter than those ccRCC patients with lower *RNASET2* expression levels (Fig. 1D). Disease-free survival (DFS) analyses revealed that the *RNASET2* expression level was correlated with DFS of ccRCC patients (Fig. 1E).

To confirm the actual expression level of *RNASET2* in cancer tissues obtained from the ccRCC patients in

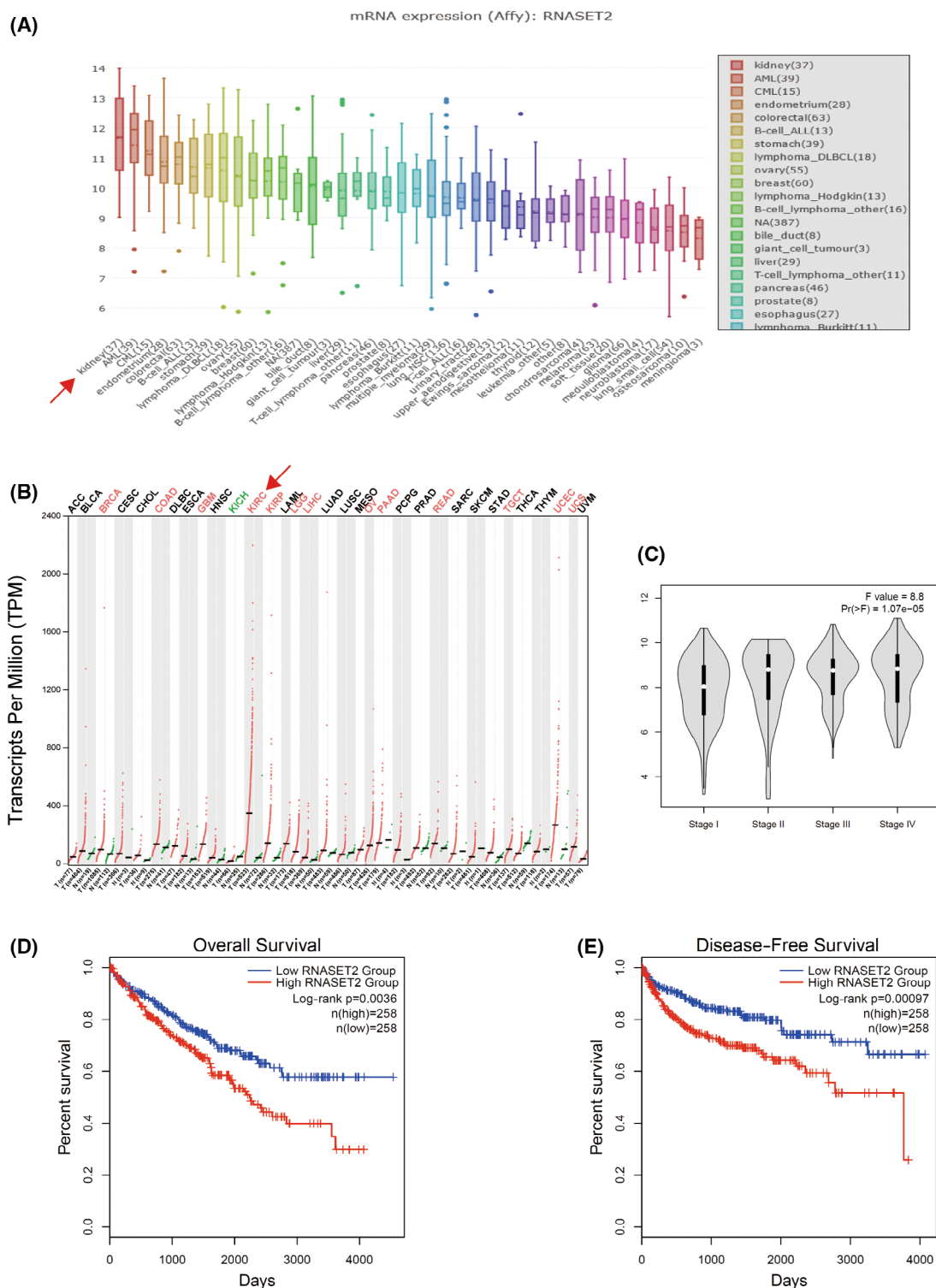


Fig. 1. *RNASET2* expression is higher in clear cell renal cell carcinoma. (A) CCLE database shows that *RNASET2* mRNA is overexpressed in kidney cancer cell lines; (B) *RNASET2* expression is significantly higher in ccRCC tissues compared with that in normal kidney tissues; (C) *RNASET2* expression in different stages of ccRCC; (D) Overall survival of ccRCC patients with different expression levels of *RNASET2* (normalized by *ACTB*), red line: high expression, blue line: low expression; (E) disease-free survival (DFS) of *RNASET2* expression in patients using TCGA datasets (normalized by *ACTB*).

our affiliated hospital, real-time quantitative RT-PCR and western blot analyses were applied, respectively, to detect both the *RNASET2* mRNA expression levels and their corresponding protein contents in ccRCC tissues. In 28 ccRCC cases, their expression levels were compared with the corresponding adjacent normal tissues (ANT). The results showed that the *RNASET2* expression levels were significantly higher in ccRCC tissues both at both the mRNA and protein expression levels (Fig. 2A,B). IHC analysis using an *RNASET2* antibody confirmed higher *RNASET2* protein expression levels than those in the ANT tissues (Fig. 2C). These results agreed with those obtained from the analyses of the TCGA datasets (Fig. 1B). On the contrary, an analysis was performed of an immunohistochemical chip (IHC chip) including 74 pairs of ccRCC tissues and their corresponding ANT. The results showed that the levels of *RNASET2* protein were much higher in the poorly differentiated (high-grade) ccRCC (Fig. 2D, E). Then, we determined whether there is a correlation between the *RNASET2* protein expression level and several key factors relevant to the patient's health status, including age, gender, tumor size, tumor grades, and clinical tumor node metastasis (cTNM) stages. The results revealed that the *RNASET2* protein expression level significantly correlated with the ccRCC grades and Tumor stages (T stages) of ccRCC patients (Table 1, Fig. 2E,F). In other words, increases in *RNASET2* protein expression levels correlated with both rises in ccRCC malignancy and *RNASET2* mRNA upregulation. Thus, these agreements strongly suggest that *RNASET2* may be a relevant molecular marker for both diagnosis and improved therapeutic management of ccRCC disease.

Upregulation of *DGAT1* and *DGAT2* expression levels in ccRCC tissues

Abnormal lipid accumulation is the most significant change in a series of different ccRCC phenotypes. On the contrary, the *RNASET2* expression levels correlated significantly with the content of triglycerides in humans [11]. We next determined whether the triglyceride synthesis was promoted in ccRCC. Differences in Oil Red O staining intensity showed that the lipid content was much higher in ccRCC tissues than that in its corresponding ANT control (Fig. 3A). Furthermore, lipid droplets completely filled the cytoplasmic area in ccRCC tissue, whereas TEM analysis showed that the mitochondrial density content waned (Fig. 3B). In general, lipid accumulation in the cells is a pathophysiological process that reflects an imbalance between lipid synthesis and lipolysis. Diacylglycerol acyltransferases,

DGAT1 and *DGAT2*, are key enzymes mediating triglyceride (TG) synthesis. They catalyze the esterification of fatty acid-CoA (FA-CoA) and promote TG synthesis from diacylglycerol (DAG). In this study, both *DGAT1* and *DGAT2* were highly expressed in ccRCC tissue compared with those in the corresponding ANT (Fig. 3C). Notably, according to the analysis of the GEPIA2 database, ccRCC patients with high *DGAT1* or *DGAT2* expression (normalized by endoplasmic reticulum marker *CANX*) usually had a shorter survival time (Fig. 3D). On the contrary, cytoplasmic *RIP140* protein is one of the critical factors relevant to triglyceride metabolism and it can promote the lipolysis process [20]. Then, *RIP140* protein was detected using IHC in ccRCC and ANT tissues. The results showed that *RIP140* protein decreased significantly in ccRCC especially in the cytoplasm (Fig. 3C), indicating that the lipolysis process in ccRCC might be inhibited. Moreover, according to the analysis of the TCGA database, a diminished expression of *RIP140* content was also correlated with shorter survival of ccRCC patients (Fig. 3D). Therefore, it is presumed that tumor cells extended their survival in advanced stages by enhancing TGs synthesis and inhibiting lipolysis through suppressing fatty acid β -oxidation.

Silence of *RNASET2* downregulates TG synthesis, cell viability, cell invasion, and cell migration of *VHL*-Deficient ccRCC cells

Both high expression levels of *RNASET2* and TG synthesis-related genes (*DGAT1* and *DGAT2*) in ccRCC prompted us to explore the relationship between them. Real-time quantitative RT-PCR assessed the mRNA expression levels of *RNASET2* in *VHL*-deficient 786-O and 769-P ccRCC cells and human proximal tubular epithelial cells HK-2 cells. *RNASET2* expression levels ranged from high to low levels in the following cells: 786-O cells > 769-P cells > HK-2 cells (Fig. 4A). *RNASET2* shRNA plasmids were transfected into 786-O or 769-P cells followed by screening with 200 μ M G418 (Fig. 4B,C). Both *DGAT1* and *DGAT2* expression levels were significantly reduced after *RNASET2* knockdown (Fig. 4D), whereas the expression levels were invariant of the lipolysis-associated *RIP140*, *ABHD5*, and *ATGL* genes (Fig. S1A). The results of Oil Red O staining showed that the intracellular lipid droplets decreased after *RNASET2* knockdown in 786-O and 769-P cells (Fig. 4E), and the lipi-red fluorescence staining was similar (Fig. 4F). To confirm the effect of *RNASET2* expression on cell proliferation, real-time cellular analysis (RTCA) using xCELLigence® Real-

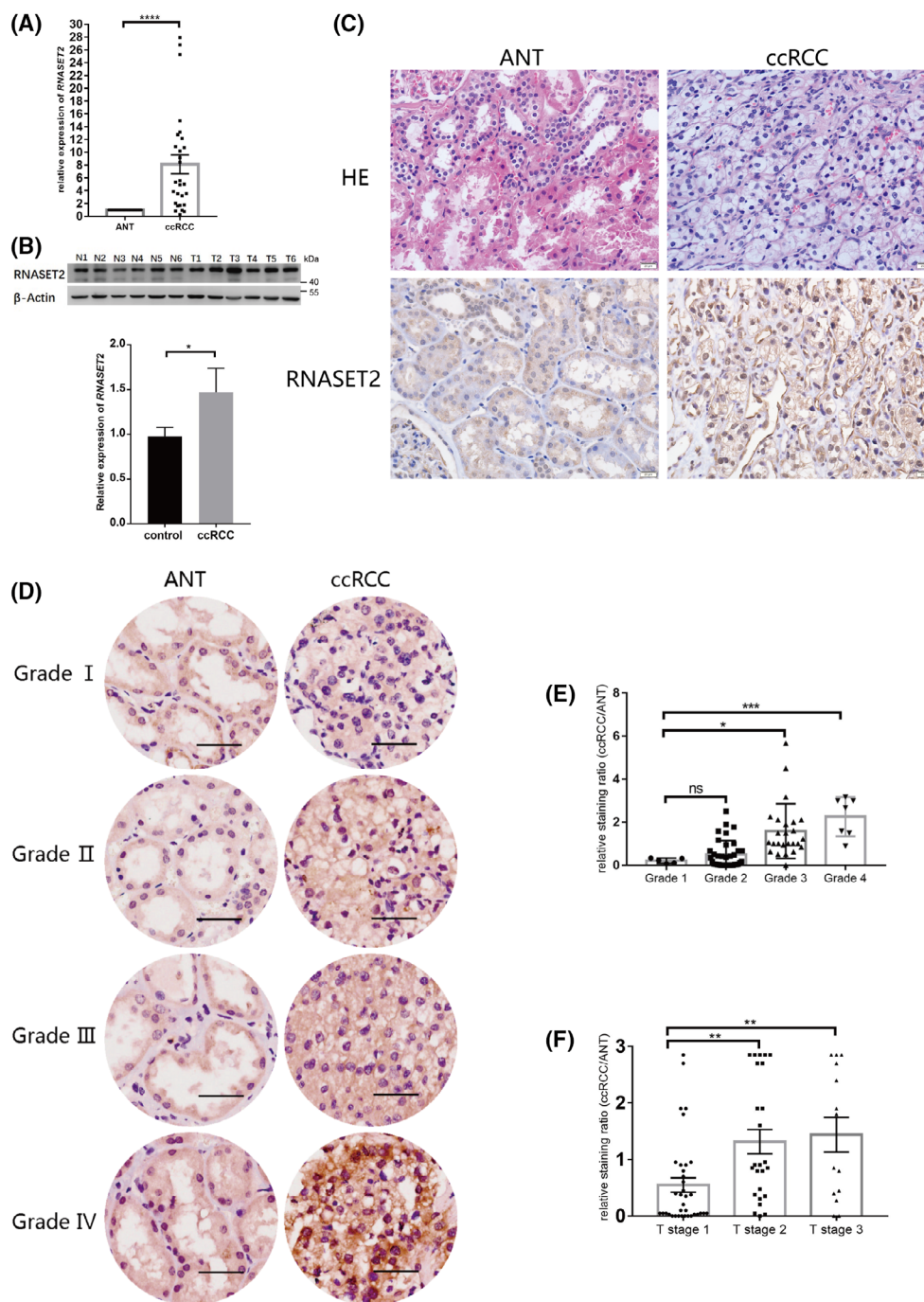


Fig. 2. *RNASET2* expression in ccRCC exceeds that in ANT. (A) The relative mRNA expression level of *RNASET2*, $n = 28$; (B) The relative protein expression level of *RNASET2* (upper, the results of western blot, N1 ~ N6: adjacent normal tissues, T1 ~ T6: ccRCC tissues; lower, analyses of western blot by gray value), $n = 28$; (C) Hematoxylin-eosin (H&E) staining and immunohistochemistry (IHC) of *RNASET2* in ccRCC and ANT, scale bars: 50 μm ; (D) IHC chip of *RNASET2* in ccRCC and ANT, scale bars: 50 μm ; (E) The relative intensity in the IHC chip of *RNASET2* expression level in different ccRCC grades, Number of different grades of cases: $n_{\text{Grade 1}} = 5$, $n_{\text{Grade 2}} = 37$, $n_{\text{Grade 3}} = 25$, $n_{\text{Grade 4}} = 7$; (F) The relative intensity in the IHC chip of *RNASET2* expression level in different ccRCC T stages, Number of different stages of cases: $n_{\text{stage 1}} = 35$, $n_{\text{stage 2}} = 25$, $n_{\text{stage 3}} = 14$. Values in bar graphs are the mean with SD. Statistical analysis was performed using the Student's *t*-test (A and B) and one-way ANOVA (E and F). * $P < 0.05$, ** $P < 0.01$, *** $P < 0.001$, **** $P < 0.0001$; ns, not significant.

Table 1. *RNASET2* expression in 74 pairs of clear cell renal cell carcinoma compared with adjacent normal tissues.

	RT2 expression in tumor		N	P-value
	Low	High		
Age (year)				
≤ 65	35	15	50	0.599
> 65	13	10	23	
Gender				
Male	34	15	49	0.794
Female	15	10	25	
Tumor size				
≤ 5 cm	18	7	25	0.134
> 5 cm	31	18	49	
Grade				
I	3	0	3	< 0.001 (***)
II	31	4	35	
III	11	17	28	
IV	4	4	8	
T stage				
1	29	8	37	0.004 (**)
2	14	10	24	
3	6	7	13	
N stage				
0	46	22	68	0.959
1	1	1	2	
2	2	1	3	
M stage				
0	49	24	73	0.059
1	0	1	1	
cTNM stage				
1	27	6	33	0.008 (**)
2	14	9	23	
3	6	8	14	
4	2	2	4	

** $P < 0.01$; *** $P < 0.001$.

Time Cell Analyzer was applied. The results showed that cell proliferation was inhibited after *RNASET2* knockdown in ccRCC cells (Fig. 4G). The traditional CCK-8 assay also showed that cell proliferation was significantly inhibited in 786-O cells after *RNASET2* knockdown (Fig. S1B). Therefore, these results directly indicated that *RNASET2* deficiency inhibited ccRCC cell growth *in vitro*.

In addition, cell invasion and migration are two important indicators for evaluating tumor progression. Both the transwell assay and the scratch wound healing assay showed that the *RNASET2* knockdown in ccRCC cells inhibited cell invasion and migration (Fig. 4H,I). Furthermore, the expression was detected of the metastasis-associated gene (*MTA2*), which is a reflection of cell migratory activity [21]. It was evaluated with the scratch wound healing assay in 786-O

cells. The result showed that *MTA2* expression level was much lower in *RNASET2* knockdown 786-O cells than that in control cells suggesting that *RNASET2* knockdown impaired cell migration (Fig. S1C). Taken together, these results suggest that *RNASET2* expression is essential for TG synthesis, and the maintenance of cell proliferation, cell invasion, and migration in *VHL*-deficient ccRCC Cells.

To further confirm the roles of *RNASET2* expression in mediating control of the expression levels of the lipids-associated genes, *RNASET2* coding sequences were transfected into 769-P ccRCC cells. The results showed that *RNASET2* overexpression significantly upregulated the key enzymes mediating triglyceride synthesis: *DGAT1* and *DGAT2* but not the lipolysis-associated gene *RIP140* (Fig. S1D). Meanwhile, RTCA measurements showed that cell proliferation was not influenced (Fig. S1E). These results strongly suggest that *RNASET2* mainly influences triglyceride synthesis rather than lipolysis in ccRCC.

HIF2 α directly regulates *RNASET2* transcription in ccRCC

VHL/HIF α pathway is one of the most important regulatory pathways in ccRCC. The tumor suppressor *VHL* targets HIF1 α and HIF2 α earmarked for proteasomal degradation [22]. Both HIF1 α and HIF2 α are hypoxia-induced transcription factors (HIF) in human cells. We evaluated whether HIF1 α regulates *RNASET2* transcription in ccRCC. Using the TCGA datasets, *RNASET2* mRNA expression was negatively correlated with *VHL* mRNA expression in ccRCC (Fig. 5A). The two main HIF α isoforms, HIF1 α and HIF2 α , have opposing effects on renal cell carcinoma biology, with HIF1 α acting as a tumor suppressor, whereas HIF2 α is an oncogene [23]. ccRCC tumors that only express HIF2 α have higher proliferation rates than those expressing both HIF1 α and HIF2 α [24]. HIF2 α is a necessary key factor for the formation of ccRCC xenografts, whereas the knockdown of HIF1 α enhances xenograft formation in cell lines expressing both HIF1 α and HIF2 α [25]. In the ccRCC 786-O and 769-P cell lines, which are both *VHL*-deficient, they display intragenic deletions of HIF1 α but express wild-type HIF2 α [25]. We found that the HIF2 α protein accumulated in the ccRCC cases based on the results of western blot analysis while the HIF1 α protein was deficient (Fig. S2). CoCl₂ exposure is a generally accepted experimental model that simulates hypoxia and inhibition of HIF α hydroxylation, which results in its accumulation in the cytoplasm. The exposure of ccRCC cells to CoCl₂, resulted in rises in the

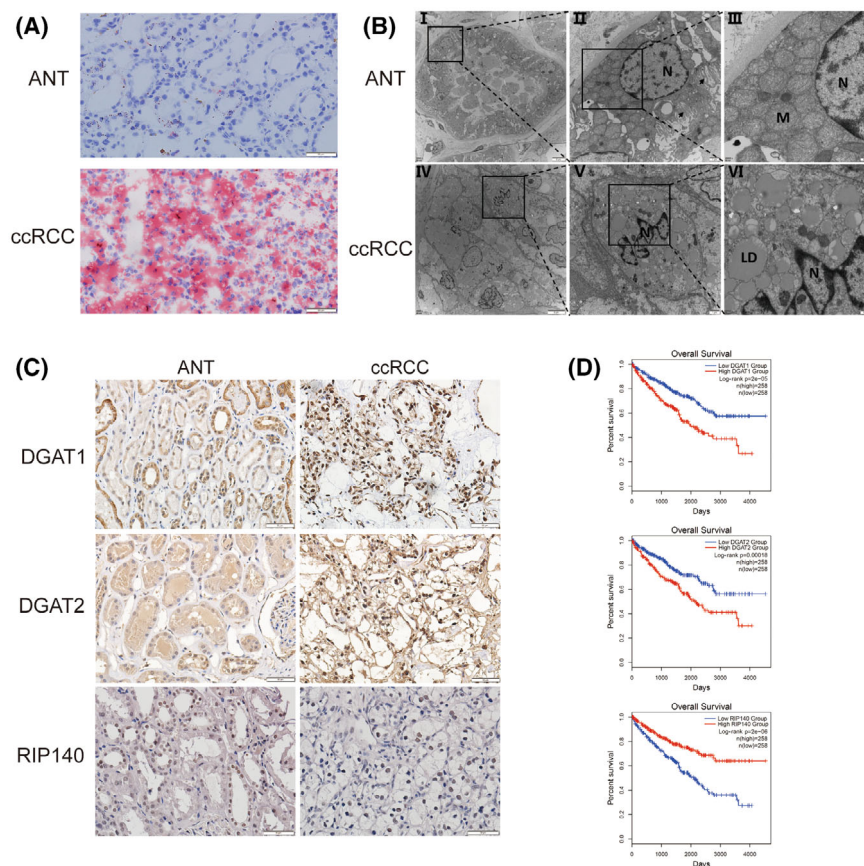


Fig. 3. High expressions of DGAT1 and DGAT2 and low expression of RIP140 in ccRCC accompanied lipid droplet accumulation. (A) Oil Red O staining monitored cytoplasmic lipid droplet accumulation in the ccRCC, scale bars, 50 μm ; (B) TEM evaluation of cytoplasmic lipid droplets that accumulated in the ccRCC, M: mitochondria; N: nucleus; LD: lipid droplet; scale bars (from left to right): 5 μm , 1 μm , and 500 nm; (C) IHC analysis compared DGAT1, DGAT2, and RIP140 expression levels in ccRCC with their corresponding values in ANT, scale bars: 50 μm ; (D) Analysis of the overall survival curves of *DGAT1*, *DGAT2*, and *RIP140* expressions base on the TCGA database (normalized by endoplasmic reticulum marker *CANX* for both *DGAT1* and *DGAT2*, *ACTB* for *RIP140*), red line: high expression; blue line: low expression.

accumulation of both the HIF2 α and the RNASET2 protein in ccRCC cells (Fig. 5B). Meanwhile, *RNASET2* mRNA expression also was significantly induced in ccRCC cells after exposure to 150 μM CoCl₂ for 24 h (Fig. 5C). Thus, we speculated that *RNASET2* is the target gene of HIF2 α . Then, chromatin immunoprecipitation-PCR (ChIP-PCR) was performed to determine whether HIF2 α interacted with the promoter of *RNASET2*. We designed the specific PCR primers to amplify a span from -278 to -187 upstream of the transcription start site (TSS) of the *RNASET2* gene (Fig. 5D), which is generally considered the promoter region. ChIP-PCR results showed that HIF2 α combined directly with the *RNASET2* promoter (Fig. 5E,F). To functionally confirm the relationship between HIF2 α and the *RNASET2* gene, we treated ccRCC cells with a HIF2 α inhibitor PT2385, which inhibits the interaction between HIF2 α and

ARNT (also known as HIF β) thus blocking the activity of HIF2 α . After exposure to different concentrations of PT2385 for 24 h, *RNASET2* transcription was detected and the results showed that treatment with 0.1 μM PT2385 significantly decreased its expression in ccRCC cells (Fig. 5G). Accordingly, *VEGF*, the proven target of HIF2 α , was also declined in parallel as expected (Fig. 5H). Therefore, these results indicated that the accumulated HIF2 α induced *RNASET2* expression in ccRCC (Fig. 5I).

Discussion

ccRCC, originating from the renal epithelial cells in the kidney cortex, does not only constitute the most frequent type of renal cancer, but it is also the second most prevalent tumor type listed in the urinary system. Its pathological identification includes that its

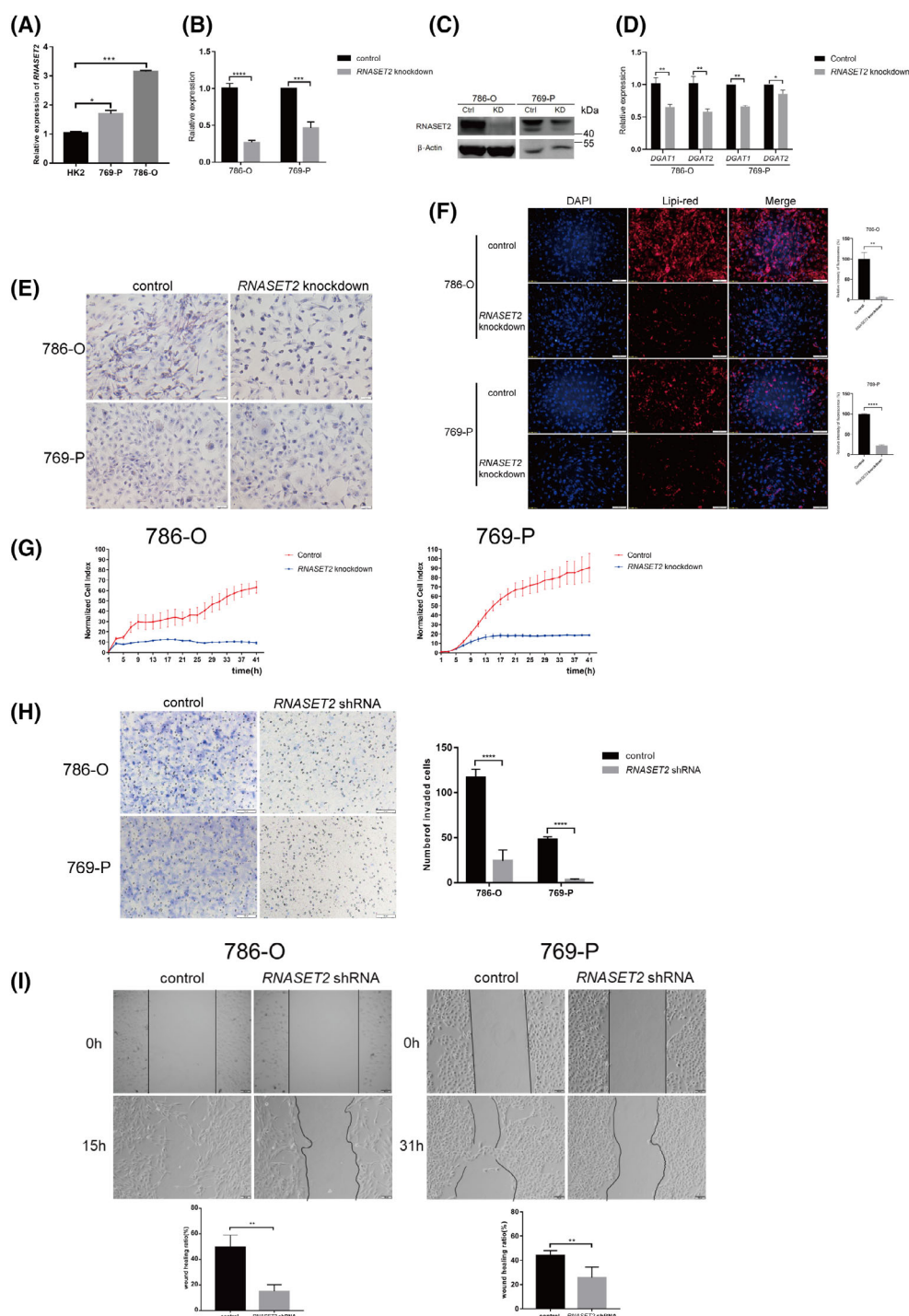


Fig. 4. *RNASET2* expression influenced the expressions of lipids-associated genes, cell proliferation, and cell migration. (A) mRNA expression level of *RNASET2* in HK-2, 769-P, and 786-O cells, respectively, $n = 3$; (B, C) *RNASET2* was knocked down in ccRCC cells by *RNASET2* shRNA, $n = 3$; (D) *RNASET2* knockdown in ccRCC cells decreased both *DGAT1* and *DGAT2* expressions, $n = 6$; (E) Oil Red O staining, scale bars: 50 μ m; (F) Assessment of lipi-red staining, scale bars: 100 μ m; (G) Real-time cell analysis (RTCA) of cell proliferation showed that it was inhibited after *RNASET2* knockdown in ccRCC cells; (H) Transwell assay to evaluate cell invasion after *RNASET2* knockdown in ccRCC cells, scale bars: 100 μ m, $n = 6$; (I) The scratch wound healing test showed that *RNASET2* deficiency inhibited the migration of ccRCC cells, scale bars: 100 μ m, $n = 6$. Values in bar graphs are the mean with SD. Statistical analysis was performed using the Student's *t*-test. * $P < 0.05$, ** $P < 0.01$, *** $P < 0.001$, **** $P < 0.0001$.

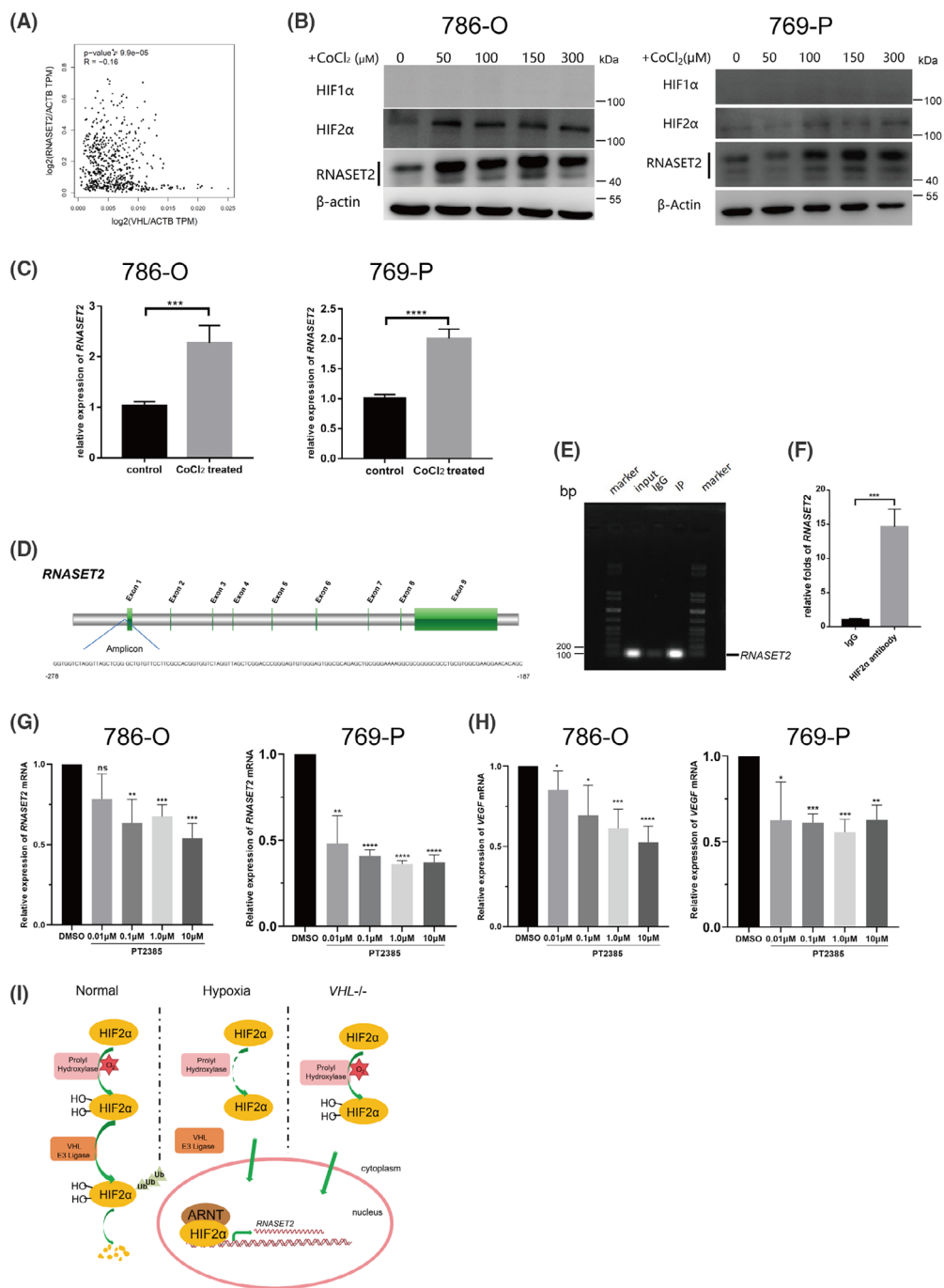


Fig. 5. HIF2 α directly interacted with *RNASET2* in ccRCC cells. (A) TCGA database analysis shows that there is a negative correlation between *RNASET2* and *VHL* expression levels, $P = 9.9 \times 10^{-5}$, $R = -0.16$; (B) Following exposure to CoCl₂ for 24 h, both HIF2 α and RNASET2 proteins were highly upregulated in 786-O and 769-P cells with HIF1 α deficiency; (C) The *RNASET2* mRNA expression level increased significantly in 786-O and 769-P cells after exposure to 150 μ M CoCl₂ for 24 h (reference gene: *ACTB*), $n = 6$; (D) Sequence of ChIP-PCR amplicon corresponding to *RNASET2* gene structure (green fragments: exons); (E, F) Fragments pulled down with HIF2 α antibody by chromatin immunoprecipitation (ChIP) was analyzed by regular PCR and quantitative real-time PCR, $n = 3$; (G) *RNASET2* transcription in 786-O and 769-P cells after exposure to different doses of PT2385 for 24 h (control: DMSO, reference gene: *ACTB*), $n = 6$; (H) *VEGF* transcription in 786-O and 769-P cells after exposure to different doses of PT2385 for 24 h (control: DMSO, reference gene: *ACTB*), $n = 6$; (I) A schematic representation showing the regulatory mechanism of *RNASET2* transcription in ccRCC. Values in bar graphs are the mean with SD. Statistical analysis was performed using the Student's t -test (C and F) and one-way ANOVA (G and H). * $P < 0.05$, ** $P < 0.01$, *** $P < 0.001$, **** $P < 0.0001$; ns, not significant.

cytoplasm is full of TGs and glycogens. With H&E staining, lipid droplets caused the cells to appear transparent [1], which was confirmed based on our results with Oil Red O staining. Moreover, our TEM analysis also revealed a high density of lipid droplets and few organelles in the cancerous cytoplasm. Due to the unique characteristics of cancerous tissue, until now there are no effective therapeutic procedures except surgery to delay its progression. One of the possible reasons for the inability to arrest its spread may stem from the huge lipid deposits in the cancerous cytoplasm [26,27]. Despite this insight, there are no novel targets that can reverse ccRCC oncogenesis. If this void can be overcome, it will undoubtedly help in diagnosing and improving the therapeutic management of ccRCC and thereby prolong survival in the early stage of its development.

For tumor biology, *RNASET2* is a multifunctional protein, which has dual-directional roles in tumor development. Some studies showed that *RNASET2* plays a role as an antitumor gene in ovarian cancer and melanoma [12,17,28]. For example, *RNASET2* expression decreased both in ovarian tumors and melanoma and it was negatively correlated with the malignancy of these tumors [12,29]. Moreover, the downregulated expression of *RNASET2* is generally associated with drug resistance in the treatment of ovarian cancer [30]. On the contrary, *RNASET2* expression is significantly higher in poorly differentiated cancer cells than that in the well-differentiated cancer cells in neuroendocrine neoplasms of the lung [14].

The current study provides suggestive evidence that *RNASET2* has the potential to become a new target for ccRCC diagnosis and therapy. In our study, the expression of *RNASET2* is significantly higher in ccRCC compared with that in the normal kidney based on TCGA dataset analyses, especially in the advanced stages of ccRCC, which was confirmed in ccRCC and ANT samples collected at our affiliated hospital. It should be emphasized that this expression pattern is somewhat different from prior reports on ovarian cancer research [12]. In addition, patients with high *RNASET2* expression in the ccRCC tissues usually had a poor prognosis compared with those with low *RNASET2* expression. Therefore, these indicate that *RNASET2* high expression in ccRCC tissues may be associated with shorter survival times in ccRCC patients. This inverse relationship is one piece of evidence supporting the notion that monitoring *RNASET2* expression levels may ultimately serve as a novel diagnostic and therapeutic target in a clinical setting.

There is other evidence suggesting the feasibility of *RNASET2* serving as a target to improve the detection

and therapeutic management of ccRCC. Haas *et al.* [11] reported that the high *RNASET2* expression in adipocytes was associated with the high content of TG in human serum. Such high levels also underlie the H&E-stained pathological transparency of the ccRCC that results from their high TG content [1]. To clarify the influences of *RNASET2* on cell lipid metabolism, we detected the expressions of key genes that are relevant to controlling the TG synthesis and lipolysis pathway. *DGAT1* and *DGAT2* are two diacylglycerol acyltransferases, which catalyze the terminal and are only the committed step in TG synthesis using diacylglycerol and fatty acyl-CoA. Moreover, *DGAT1* is highly expressed in the intestine and it can promote fatty acid (FA) absorption. *DGAT1* is also expressed in the testis, liver, and adipose tissues, while *DGAT2* is highly expressed in the liver and adipose tissues, but it is expressed at low levels in the intestine [31]. Cytoplasmic Rip140 can interact with perilipin to regulate lipolysis [20]. In the current research, we found that both *DGAT1* and *DGAT2* expressions were upregulated, but *RIP140* was downregulated in ccRCC tissues compared with those in the ANT tissues.

We determined whether there is an association between changes in these lipids-associated genes and alterations in *RNASET2* expression levels. Our results documented that the expression of *DGAT1* and *DGAT2* decreased significantly in ccRCC cells when *RNASET2* was knocked down, whereas when *RNASET2* was overexpressed, the expression of *DGAT1* and *DGAT2* increased significantly. However, modulation of the *RNASET2* expression level did not affect changes in the *RIP140* expression levels. These results strongly confirmed that *RNASET2* can regulate the lipids-synthesis genes *DGAT1* and *DGAT2* expression, which leads to increases in triglyceride synthesis and lipid droplet formation in ccRCC cells. Excess amounts of free fatty acids (FFAs) and diacylglycerols (DAGs) in the cell usually lead to lipotoxicity [32], while lipid droplets are generally considered as the central antilipotoxic organelles that control lipotoxicity by sequestering these potentially toxic lipids into inert triglycerides [32–34]. Herein, we speculate that *RNASET2* promoted the synthesis of TGs to resist lipotoxicity in ccRCC.

Moreover, we also investigated the possible pathways relevant to the function of *RNASET2* protein in *VHL*-deficient 786-O cells through immunoprecipitation-mass spectrometry (IP-MS; Fig. S3). The results of IP-MS showed that the proteins that interacted with *RNASET2* were involved in various signaling pathways in 786-O cells. Besides ribosome proteins, numerous other proteins are involved in the metabolic pathways

especially in fatty acid metabolism in the MS list. They include fatty acid-binding protein 5 (FABP5), elongation of very long-chain fatty acid-like 1 (ELOVL1), acyl-CoA synthetase long-chain family member proteins (ACSL3 and ACSL4), and metastasis-associated protein MTA2. Lv *et al.* [35] reported that FABP5 expression was significantly upregulated in ccRCC and patients with a high expression level of FABP5 were correlated with tumor metastasis classifications that were also predicted to have poor survival. ELOVL1 is an enzyme elongating saturated and monounsaturated fatty acids [36]. Silencing *ELOVL1* can reduce the lipidomic profiles and viability of breast cancer cells [37]. In recent years, several studies demonstrated that ferroptosis was involved in the development of varied tumors. ACSL3 and ACSL4 can incorporate polyunsaturated fatty acids (PUFAs) into phospholipids, which is a critical step in ferroptosis [38]. ACSL3 is highly expressed in human lung cancer specimens and it can promote cancer initiation [39]. Oleic acid can protect melanoma cells from ferroptosis in an ACSL3-dependent manner [40]. ACSL4 is upregulated in many cancers, including liver cancer, prostate cancer, breast cancer, and colon cancer [26]. In addition, MTA2 is a metastasis-associated protein, which plays some vital roles during the metastasis of tumors [41,42]. In the current study, there is a correlation between *MTA2* expression and *RNASET2* expression, as well as cancer cell migration in ccRCC cells. Accordingly, *RNASET2* may have some special effects on the development and metastasis of ccRCC through interacting with these target proteins.

Hypoxic status is one of the crucial factors controlling malignant tumor development and metastasis. Uccella *et al.* [14] reported that the expression of the *RNASET2* protein was induced in the *HIF1 α* -transfected human breast cancer-derived MCF7 cell line. However, *HIF1 α* activity is often deficient because of the chromosomal 14q loss in some ccRCC cases [43], whereas *HIF2 α* is highly expressed in ccRCC due to *VHL* deficiency [24]. To investigate the mechanism involved in the regulation of *RNASET2* transcription, we performed ChIP experiments in the ccRCC cell line 786-O characterized as having a *VHL* and *HIF1 α* deficiency like most ccRCC cases. The ChIP-PCR results showed that the transcription of *RNASET2* is upregulated by *HIF2 α* directly, which is accumulated in *VHL*-deficient ccRCC cells.

VHL is one of the most important tumor suppressor genes in humans. Some research documented that the *VHL* gene is a crucial factor in the pathogenesis of ccRCC. For instance, there are *VHL* mutations that include loss of chromosome 3p25 where the *VHL* gene is located, or promoter hypermethylation of the *VHL*

gene in nearly 80% of ccRCC cases [44–47]. *VHL* deficiency leads to the accumulation of *HIF1 α* and *HIF2 α* , which are hypoxia-inducible factors. Although *HIF2 α* has a far greater role in ccRCC, its role in tumorigenesis has been less extensively studied than that of *HIF1 α* [48]. Our results employing TCGA database analysis also showed that there was a negative correlation between *RNASET2* and *VHL* expression levels in ccRCC cells. *VHL* deficiency-induced *HIF1 α* accumulation can be integrated with ARNT in the cells, and then, the integrated complex is transferred into the cell nucleus to activate the transcription of the target genes or downstream genes in the pathways. They include MMP9, VEGF, and PDGF, which can promote both cancer cell proliferation and metastasis [49–51]. Thus, most of the drugs applied in the clinics generally target the *VHL/HIF1 α /VEGF* signaling pathway axes. For example, Sorafenib and Sunitinib are two drugs that have been approved for the therapeutic management of advanced-stage renal cell cancer, which can depress the development of renal cell cancer by inhibiting VEGFR, PDGFR, and FLT3 expression levels [3,52]. Bevacizumab, an anti-VEGF recombination monoclonal antibody, can work together with interferon in treating ccRCC [53]. Besides, *HIF2 α* is another critical therapeutic target for ccRCC treatment. Extensive biochemical efforts resulted in optimizing PT2385, a leading *HIF2 α* inhibitor [54], which was later modified and improved and redesignated as PT2977, a second-generation inhibitor (now known as ‘MK-6482’) [55]. Both of these two inhibitors can block the transcription of *HIF2 α* -targeted genes, including *VEGFA*, *CCND1*, and *SLC2A1* [56,57]. In the current study, we demonstrated that *RNASET2* is also the target gene of *HIF2 α* in ccRCC. Therefore, it is suggested that the *HIF2 α* inhibitors may also block the transcription of *RNASET2* gene.

In conclusion, the current research shows that overexpression of *RNASET2* is associated with increases in ccRCC progression, especially in poorly differentiated tumors. On the contrary, a negative correlation exists between *RNASET2* mRNA and *VHL* mRNA expressions. Meanwhile, increases in transcription factor *HIF2 α* , in turn, upregulate *RNASET2* expression in ccRCC. Moreover, the results show that increases in *RNASET2* expression promote increases in gene expression of *DGAT1* and *DGAT2*, which account for rises in both TGs syntheses. These effects ultimately protect the cancer cells and promote cell migration in ccRCC. Therefore, this research provides valuable insight for further etiological clarification of factors controlling ccRCC progression. This endeavor is likely to identify new therapeutic targets such as *RNASET2* in the clinics. However, although we elucidated the

signaling pathway through which changes in *RNA-SET2* expression levels modulate ccRCC oncogenesis *in vitro*, some important experiments *in vivo*, such as tumor xenograft in nude mice, are still needed to clarify how such changes affect ccRCC oncogenesis.

Materials and methods

Patient specimens and cell lines

This study enrolled subjects visiting the Department of Urology, Shanghai Ruijin Hospital between September 2018 and August 2021. Their clear cell renal cell carcinoma (ccRCC) tissues and adjacent normal tissues (ANT) were obtained during the surgical operation. The study conformed to the standards set by the Declaration of Helsinki was approved by the Ethics Committee of Ruijin Hospital, Shanghai Jiao Tong University School of Medicine, China (approval number: 2018-381). All subjects gave written informed consent before their participation. Twenty-eight pairs of samples including both ccRCC and ANT tissues were collected after surgery for the following experiments. ccRCC cell lines 786-O and 769-P and human proximal tubular epithelial cell line HK-2 were provided by the National Collection of Authenticated Cell Cultures. 786-O cells and 769-P cells were immediately cultured in RPMI1640 medium (Gibco, Waltham, MA, USA) and HK-2 cells were cultured in DME/F12 medium (Gibco) when the cell lines were obtained. All the culture media contained 10% fetal bovine serum (FBS), 100 U·mL⁻¹ penicillin, and 100 µg·mL⁻¹ streptomycin, and the cultured cells were kept in 95% humidity and 37 °C 5% CO₂ incubator (Thermo, Waltham, MA, USA).

RNA isolation and quantitative Real-Time PCR

Total RNA was extracted with the TRIzol reagent (Invitrogen, Carlsbad, CA, USA). cDNA synthesis of genes was performed with a PrimeScript™ RT Master Mix (Takara, Shiga, Japan). Subsequently, quantitative real-time PCR was carried out with TB Green® Premix Ex Taq™ (Tli RNaseH Plus) mix (Takara). The PCR system was successfully run in Applied Biosystem 7500 (ABI, Waltham, MA, USA). All the primers for real-time RT-PCR analyses were designed by PRIMER PREMIER 6 software (Premier Inc., Palo Alto, CA, USA), which is shown in Table S1.

Protein purification and western blot

Tissues or cells were lysed using RIPA lysis buffer supplemented with protease inhibitors (Yeasen, Shanghai, China). Equal amounts of total protein lysate (30 µg per sample) were separated by 4 ~ 12% SDS/PAGE and then were transferred onto a PVDF membrane (Millipore, Billerica, MA, USA) by a wet transfer apparatus (Bio-Rad, Hercules, CA, USA). After that, the membranes were blocked with 5% BSA in TBS-T

(Tris-HCl/NaCl solution with 1% tween 20) and probed with primary antibodies (dilution 1 : 1000) overnight at 4 °C (RNASTE2: ab107313, Abcam, Cambridge, UK; HIF2α: NB100-122, Novus, Centennial, CO, USA) while β-actin (cat: 4967, CST, Beverly, MA, USA) was used as the internal control (dilution 1 : 1000), followed by incubation of corresponding horseradish peroxidase-linked secondary antibody (CST) for 2 h at room temperature. Finally, the membranes were reacted with ECL western blot substrate kit (Millipore) before exposure with ImageQuant LAS4000 (GE, Chicago, IL, USA).

Immunohistochemistry (IHC) staining

IHC staining was performed after dewaxing and rehydrating paraffin-embedded tissue sections. Subsequently, antigen retrieval was done by boiling the tissue for 15 min in 10 mM citrate buffer, pH 6.0. Then, the Histostain LAB-SA Detection kits (Invitrogen, OR, USA) were applied according to the manufacturer's instructions, and the sections were stained using DAB, while nuclei were counterstained with hematoxylin. After the sample was washed with PBS buffer thrice, the digital images were captured under a microscope (Olympus BX53) equipped with a DP74 40× objective (Olympus, Tokyo, Japan).

Oil red O staining

The Oil Red O staining was followed by the Modified Oil Red O staining kit protocol (Solarbio, Beijing, China). Briefly, the frozen sections or cell slides were fixed in 10% formalin for 10 min and washed with distilled water, and then immersed in 60% isopropanol for 30 s. Then, the slides were immersed into the modified Oil Red O staining buffer immediately for 10 min. Next, the superfluous staining buffer was removed, and then, the slides were washed with 60% isopropanol and distilled water, respectively. Meanwhile, the nuclei were counterstained with hematoxylin for 1 min and washed with distilled water. Finally, the slides were sealed with gelatin and the digital images were captured under a microscope (Olympus) equipped with a DP74 40× objective (Olympus).

Lipi-red staining

Lipi-red staining (DOJINDO, Kumamoto, Japan) evaluated the extent of lipid droplet accumulation. G418 (200 µg·mL⁻¹) exposure was performed to screen for cell stability. The cells were plated and expanded on slides until they reached a density of about 70% at 37 °C and 5% CO₂. One micromolar lipi-red work solution was added and incubated at 37 °C 5% CO₂ for 30 min. The cells were washed with PBS thrice and then covered with the antifade mounting solution containing DAPI (Yeasen). The pictures were captured under a microscope (Olympus).

Cell viability assay

The Cell Counting Kit-8 (CCK-8; DOJINDO) evaluated the effect of *RNASET2* knockdown on 786-O cell viability. Stable screening cells were isolated by exposure to 200 $\mu\text{g}\cdot\text{mL}^{-1}$ G418. The cells were expanded until they reached a cell density of about 70% at 37 °C 5% CO_2 . CCK-8 (5 $\text{mg}\cdot\text{mL}^{-1}$) was added and the cells were incubated at 37 °C under 5% CO_2 for 1 h. Optical density (OD) was read on a microplate reader at an absorbance value of 450 nm (Thermo). Three independent experimental replicates were performed.

Transmission electron microscopy (TEM) analysis

Tissues for TEM were prepared just following the protocols [58]. Briefly, small pieces of ccRCC tissues and ANT tissues were immersed in 2.5% glutaraldehyde solubilized in 0.1 M phosphate buffer (pH 7.4) for 1 day. The tissues were then fixed in 1% osmium tetroxide and dehydrated through a graded ethanol series, and embedded in Epon 618 (TAAB Laboratories Equipment, Berks, UK). Ultra-thin sections (70 ~ 90 nm) sliced from the tissues were stained with lead citrate and uranyl acetate and then examined at 100 kV with a Philips CM-120 (Philips, Eindhoven, the Netherlands).

shRNA plasmids transfection

To construct shRNA plasmids, the shRNA oligo for *shRNASET2* (forward sequence 5'-GCAAGAGAAUU CACAAACUGCAGC-3' and reverse sequence 5'-GCUG CAGUUUGUGAAUUUCUCUUGCUU-3') and control shRNA (forward sequence 5'-CUUCCUCUCUUUCUCU CCCUUGUGA-3' and reverse sequence 5'-UCACAAGGG AGAGAAAGAGAGGAAGGA-3') [28] were cloned into the pGPU6/GFP/Neo vector (GenePharma, Shanghai, China) according to the manufacturer's instruction. ccRCC cell line 786-O cells or 769-P cells were transfected with *RNASET2* shRNA plasmids or control shRNA plasmids using HighGene transfection reagent (Abclonal, Wuhan, China) and selected for 2 weeks in 500 $\mu\text{g}\cdot\text{mL}^{-1}$ Geneticin (G418; Selleck, Houston, TX, USA). Subsequently, the selected cells were cultured in 200 $\mu\text{g}\cdot\text{mL}^{-1}$ G418.

Real-Time cell analysis (RTCA)

A real-time cell analysis experiment is a more accurate method to estimate cell states using micro-electronic biosensor technology. This method detects time-dependent changes in cell proliferation in real time. Briefly, 50 μL of cell culture medium was added to each well of the RTCA plate to establish a baseline. Then, 100 μL of a cell suspension containing about 5000 cells was added to each well. Finally, cells were auto-scanned using RTCA xCELLigence system (ACEA Biosciences, San Diego, CA, USA) every 15 min.

Scratch wound healing assay

To measure cell migration, a scratch wound healing assay was performed. ccRCC cells transfected with *RNASET2* shRNA-pGPU6/GFP/Neo plasmids and scramble sequence-pGPU6/GFP/Neo plasmids (control) were planted in 6-well plates with horizontal lines predrawn on the plate back, respectively. Cells grew to form a monolayer at 37 °C 5% CO_2 under normoxic conditions overnight. Subsequently, cells were removed from the plates by scratching their surfaces with 10 μL pipette tips to create vertical wounds perpendicular to the drawn horizontal lines. Wells were washed thrice with PBS to remove the floating cells, and then, fresh RPMI1640 medium without FBS was added to the wells. The transfected cells 786-O and 769-P were incubated at 37 °C, 5% CO_2 conditions for 15 and 31 h, respectively, depending on their migration rate. Then, the photographs were captured under the inverted microscope (Olympus). Five fields were randomly selected and the scratch wound healing was analyzed with IMAGEJ software (NIH, Bethesda, MD, USA).

Transwell assay

The upper transwell chamber was coated with a cell suspension containing $10 \times 10^4\cdot\text{mL}^{-1}$ cells and Matrigel 200 μL with serum-free RPMI-1640 medium was added to this chamber, and 600 μL RPMI-1640 medium containing 20% fetal bovine serum was added to the lower chamber, respectively. The upper chamber was carefully immersed in the lower chamber liquid. A plate consisting of 24-well transwell chambers was incubated at 37 °C under 5% CO_2 for 24 h. The liquid was removed from the upper chamber and washed thrice with 600 μL PBS. After staining, the upper chamber with crystal violet was observed under a microscope and photographed (Olympus). Three independent experimental replicates were performed.

CoCl₂ treatment

ccRCC cell line 786-O cells or 769-P cells were planted in a 6-well plate and incubated at 37 °C, 5% CO_2 overnight. Then, the cells were incubated with fresh RPMI1640 media containing 10% FBS and treated with 0, 50, 100, 150, and 300 μM CoCl₂, respectively, for 24 h. Cells were harvested and washed thrice with PBS buffer, and then applied for use in various experiments.

PT2385 treatment

Cells were placed in a 6-well plate and incubated at 37 °C under 5% CO_2 overnight. Then, the medium was replaced with fresh RPMI1640 medium containing 10% FBS and exposed to 0.01, 0.1, 1.0, and 10 μM PT2385, respectively, for 24 h (control: DMSO). Cells were harvested and

washed thrice with PBS buffer and then applied for use in various experiments.

Coimmunoprecipitation and mass spectrometry (MS)

For MS analysis, coimmunoprecipitation was performed according to Capture™ IP & Co-IP Kit (Takara). Briefly, 786-O cells were washed with cold PBS once the culture media was removed. The cellular lysate was prepared using lysis/equilibration buffer and incubated on ice for 15 min and then centrifuged at $17\,000 \times g$ for 10 min at 4 °C. The supernatant was transferred into a new 1.5 mL tube and incubated with RNASET2 antibody on a rotator at 4 °C overnight. Next, 100 μ L of lysis buffer was added to a spin column in a provided collection tube for equilibration, and then, the tube was centrifuged at $1000 \times g$ for 1 min at room temperature. The column was placed into a new collection tube following loading of the protein-RNASET2 antibody mixture and centrifuged at $1000 \times g$ for 1 min at room temperature. Finally, the sample flow-through was saved for MS analysis. The MS analysis was performed with the Orbitrap Fusion Lumos spectrometer (ThermoFisher Scientific). The peak list MS features were annotated using KEGG (Kyoto Encyclopedia of Genes and Genomes) pathway analysis.

Chromatin immunoprecipitation-PCR (ChIP-PCR)

786-O cells were cross-linked with formaldehyde, and chromatin was isolated and sheared by the Bioruptor Sonication System (Diagenode, Liege, Belgium) to obtain an average fragment size of 200 ~ 1000 bp. Sheared chromatin fragments were incubated with the anti-HIF2 α antibody (NB100-122; Novus). Meanwhile, an equal concentration of nonspecific IgG was used as the negative control. The immunoprecipitated protein-DNA complex was obtained using protein A/G immunomagnetic beads, and DNA was isolated by the standard phenol/chloroform/ethanol precipitation method. PCR was amplified with the *RNASET2* primers (forward primer 5'-GGTGGTCTAGGTTAGCTC GG-3'; reverse primer: 5'-GCTGTGTTCCCTTCGCCAC-3'). The amplicon was corresponding to the -278 to -187 region located the upstream of *RNASET2* transcript start site (TSS).

Statistical analysis

All data were analyzed using the SAS 8.2 software (SAS Institute Inc., Cary, NC, USA), and results are presented as mean \pm SD. The paired *t*-test or Student's *t*-test was used where appropriate. A one-way analysis of variance test was used assuming a two-tailed hypothesis with $P < 0.05$. The survival curves were plotted using the

Kaplan–Meier method, and the differences were assessed using the log-rank test. $P < 0.05$ was considered a statistically significant difference. The gray values of western blot bands were analyzed by IMAGEJ software (NIH). In addition, the survival time of subjects was calculated from the date of surgery to the date of death. Statistical analysis of survival time was carried out using the Kaplan–Meier survival test. Meanwhile, the cancer genome atlas program (TCGA) and the online tool GEPIA2 (gepia2.cancer-pku.cn) were also applied to analyze the survival curve.

Acknowledgements

The authors thank Ms Rong Fu (Core Facility of Basic Medical Sciences) for her technical assistance in the flow cytometry assay. The authors are very appreciative of the support provided by Prof Peter Reinach for his extensive and detailed support in improving the manuscript writing style. This research was supported by grants from the National Natural Science Foundation of China (No. 82071694, 81971437, and 81571487) and the Science and Technology Commission of Shanghai Municipality (No. 21140904000 and 201409005800).

Conflict of interest

The authors declare no conflict of interest.

Author contributions

YQ, LZ, LJ, YLo, and YH performed all the experiments. JD, SZ, and SL contributed to reagents and material preparation. YQ analyzed the data and wrote the manuscript. ZD, JZ, and YLi contributed to the planning and supervising of the study and revision of the manuscript.

Data accessibility

The data that support the findings of this study are available upon request from the corresponding author. The data are not publicly available due to privacy or ethical restrictions.

References

- Rini BI, Campbell SC and Escudier B (2009) Renal cell carcinoma. *Lancet* **373**, 1119–1132.
- Yuan L, Zeng G, Chen L, Wang G, Wang X, Cao X, Lu M, Liu X, Qian G, Xiao Y *et al.* (2018) Identification of key genes and pathways in human clear cell renal cell carcinoma (ccRCC) by co-expression analysis. *Int J Biol Sci* **14**, 266–279.

- 3 Hsieh JJ, Purdue MP, Signoretti S, Swanton C, Albiges L, Schmidinger M, Heng DY, Larkin J and Ficarra V (2017) Renal cell carcinoma. *Nat Rev Dis Primers* **3**, 17009–17050.
- 4 Cuadros T, Trilla E, Sarró E, Vilà MR, Vilardell J, de Torres I, Salcedo M, López-Hellin J, Sánchez A, Ramón Y *et al.* (2014) HAVCR/KIM-1 activates the IL-6/STAT-3 pathway in clear cell renal cell carcinoma and determines tumor progression and patient outcome. *Cancer Res* **74**, 1416–1428.
- 5 van der Mijl JC, Mier JW, Broxterman HJ and Verheul HM (2014) Predictive biomarkers in renal cell cancer: insights in drug resistance mechanisms. *Drug Resist Updat* **17**, 77–88.
- 6 Quan C, Ren YQ, Xiang LH, Sun LD, Xu AE, Gao XH, Chen HD, Pu XM, Wu RN, Liang CZ *et al.* (2010) Genome-wide association study for vitiligo identifies susceptibility loci at 6q27 and the MHC. *Nat Genet* **42**, 614–618.
- 7 Campomenosi P, Salis S, Lindqvist C, Mariani D, Nordström T, Acquati F and Taramelli R (2006) Characterization of RNASET2, the first human member of the Rh/T2/S family of glycoproteins. *Arch Biochem Biophys* **449**, 17–26.
- 8 Vidalino L, Monti L, Haase A, Moro A, Acquati F, Taramelli R and Macchi P (2012) Intracellular trafficking of RNASET2, a novel component of P-bodies. *Biol Cell* **104**, 13–21.
- 9 Liu P, Huang J, Zheng Q, Xie L, Lu X, Jin J and Wang G (2017) Mammalian mitochondrial RNAs are degraded in the mitochondrial intermembrane space by RNASET2. *Protein Cell* **8**, 735–749.
- 10 Scaldaferrri D, Bosi A, Fabbri M, Pedrini E, Inforzato A, Valli R, Frattini A, De Vito A, Noonan DM, Taramelli R *et al.* (2018) The human RNASET2 protein affects the polarization pattern of human macrophages in vitro. *Immunol Lett* **203**, 102–111.
- 11 Haas BE, Horvath S, Pietiläinen KH, Cantor RM, Nikkola E, Weissglas-Volkov D, Rissanen A, Civelek M, Cruz-Bautista I, Riba L *et al.* (2012) Adipose co-expression networks across Finns and Mexicans identify novel triglyceride-associated genes. *BMC Med Genomics* **5**, 61–70.
- 12 Acquati F, Morelli C, Cinquetti R, Bianchi MG, Porrini D, Varesco L, Gismondi RR, Talevi S, Possati L, Magnanini C *et al.* (2001) Cloning and characterization of a senescence inducing and class II tumor suppressor gene in ovarian carcinoma at chromosome region 6q27. *Oncogene* **20**, 980–988.
- 13 Zeng Z, Zhang X, Li D, Li J, Yuan J, Gu L and Xiong X (2020) Expression, location, clinical implication, and bioinformatics analysis of RNASET2 in gastric adenocarcinoma. *Front Oncol* **10**, 836–850.
- 14 Uccella S, La Rosa S, Scaldaferrri D, Monti L, Maragliano R, Sorrenti E, Gariboldi M, Taramelli R, Sessa F and Acquati F (2018) New insights into hypoxia-related mechanisms involved in different microvascular patterns of bronchopulmonary carcinoids and poorly differentiated neuroendocrine carcinomas. Role of ribonuclease T2 (RNASET2) and HIF-1 α . *Hum Pathol* **79**, 66–76.
- 15 Turconi G, Scaldaferrri D, Fabbri M, Monti L, Lualdi M, Pedrini E, Gribaldo L, Taramelli R and Acquati F (2016) RNASET2 silencing affects miRNAs and target gene expression pattern in a human ovarian cancer cell model. *Int J Oncol* **49**, 2637–2646.
- 16 Ji M, Zhao Z, Li Y, Xu P, Shi J, Li Z, Wang K, Huang X and Liu B (2021) FBXO6-mediated RNASET2 ubiquitination and degradation governs the development of ovarian cancer. *Cell Death Dis* **12**, 317–327.
- 17 Monti L, Rodolfo M, Lo Russo G, Noonan D, Acquati F and Taramelli R (2008) RNASET2 as a tumor antagonizing gene in a melanoma cancer model. *Oncol Res* **17**, 69–74.
- 18 Li H, Ning S, Ghandi M, Kryukov GV, Gopal S, Deik A, Souza A, Pierce K, Keskula P, Hernandez D *et al.* (2019) The landscape of cancer cell line metabolism. *Nat Med* **25**, 850–860.
- 19 Tang Z, Kang B, Li C, Chen T and Zhang Z (2019) GEPIA2: an enhanced web server for large-scale expression profiling and interactive analysis. *Nucleic Acids Res* **47**, 556–560.
- 20 Ho PC, Chuang YS, Hung CH and Wei LN (2011) Cytoplasmic receptor-interacting protein 140 (RIP140) interacts with perilipin to regulate lipolysis. *Cell Signal* **23**, 1396–1403.
- 21 Kumar R, Wang RA and Bagheri-Yarmand R (2003) Emerging roles of MTA family members in human cancers. *Semin Oncol* **5**, 30–37.
- 22 Maxwell PH, Wiesener MS, Chang GW, Clifford SC, Vaux EC, Cockman ME, Wykoff CC, Pugh CW, Maher ER and Ratcliffe PJ (1999) The tumour suppressor protein VHL targets hypoxia-inducible factors for oxygen-dependent proteolysis. *Nature* **399**, 271–275.
- 23 Schödel J, Grampp S, Maher ER, Moch H, Ratcliffe PJ, Russo P and Mole DR (2016) Hypoxia, hypoxia-inducible transcription factors, and renal cancer. *Eur Urol* **69**, 646–657.
- 24 Gordan JD, Lal P, Dondeti VR, Letrero R, Parekh KN, Oquendo CE, Greenberg RA, Flaherty KT, Rathmell WK, Keith B *et al.* (2008) HIF-1 α effects on c-Myc distinguish two subtypes of sporadic VHL-deficient clear cell renal carcinoma. *Cancer Cell* **14**, 435–446.
- 25 Shen C, Beroukhi R, Schumacher SE, Zhou J, Chang M, Signoretti S and Kaelin WG Jr (2011) Genetic and functional studies implicate HIF1 α as a 14q kidney cancer suppressor gene. *Cancer Discov* **1**, 222–235.

- 26 Butler LM, Perone Y, Dehairs J, Lupien LE, de Laat V, Talebi A, Loda M, Kinlaw WB and Swinnen JV (2020) Lipids and cancer: emerging roles in pathogenesis, diagnosis and therapeutic intervention. *Adv Drug Deliv Rev* **159**, 245–293.
- 27 Cotte AK, Aires V, Fredon M, Limagne E, Derangère V, Thibaudin M, Humblin E, Scagliarini A, de Barros JP, Hillon P *et al.* (2018) Lysophosphatidylcholine acyltransferase 2-mediated lipid droplet production supports colorectal cancer chemoresistance. *Nat Commun* **9**, 322–337.
- 28 Gonsky R, Fleshner P, Deem RL, Biener-Ramanujan E, Li D, Potdar AA, Bilsborough J, Yang S, McGovern DPB and Targan SR (2017) Association of ribonuclease T2 gene polymorphisms with decreased expression and clinical characteristics of severity in Crohn's disease. *Gastroenterology* **153**, 219–232.
- 29 Acquati F, Bertilaccio S, Grimaldi A, Monti L, Cinquetti R, Bonetti P, Lualdi M, Vidalino L, Fabbri M, Sacco MG *et al.* (2011) Microenvironmental control of malignancy exerted by *RNASET2*, a widely conserved extracellular RNase. *Proc Natl Acad Sci USA* **108**, 1104–1109.
- 30 Yin F, Liu L, Liu X, Li G, Zheng L, Li D, Wang Q, Zhang W and Li L (2014) Downregulation of tumor suppressor gene ribonuclease T2 and gametogenetin binding protein 2 is associated with drug resistance in ovarian cancer. *Oncol Rep* **32**, 362–372.
- 31 Yen CL, Stone SJ, Koliwad S, Harris C and Farese RV Jr (2008) Thematic review series: glycerolipids. DGAT enzymes and triacylglycerol biosynthesis. *J Lipid Res* **49**, 2283–2301.
- 32 Petan T, Jarc E and Jusović M (2018) Lipid droplets in cancer: guardians of fat in a stressful world. *Molecules* **23**, 1941–1981.
- 33 Jarc E, Kump A, Malavašič P, Eichmann TO, Zimmermann R and Petan T (2018) Lipid droplets induced by secreted phospholipase A2 and unsaturated fatty acids protect breast cancer cells from nutrient and lipotoxic stress. *Biochim Biophys Acta Mol Cell Biol Lipids* **1863**, 247–265.
- 34 Listenberger LL, Han X, Lewis SE, Cases S, Farese RV Jr, Ory DS and Schaffer JE (2003) Triglyceride accumulation protects against fatty acid-induced lipotoxicity. *Proc Natl Acad Sci USA* **100**, 3077–3082.
- 35 Lv Q, Wang G, Zhang Y, Han X, Li H, Le W, Zhang M, Ma C, Wang P and Ding Q (2019) FABP5 regulates the proliferation of clear cell renal cell carcinoma cells via the PI3K/AKT signaling pathway. *Int J Oncol* **54**, 1221–1232.
- 36 Jakobsson A, Westerberg R and Jakobsson A (2006) Fatty acid elongases in mammals: their regulation and roles in metabolism. *Prog Lipid Res* **45**, 237–249.
- 37 Hilvo M, Denkert C, Lehtinen L, Müller B, Brockmöller S, Seppänen-Laakso T, Budczies J, Bucher E, Yetukuri L, Castillo S *et al.* (2011) Novel theranostic opportunities offered by characterization of altered membrane lipid metabolism in breast cancer progression. *Cancer Res* **71**, 3236–3245.
- 38 Killion EA, Reeves AR, El Azzouny MA, Yan QW, Surujon D, Griffin JD, Bowman TA, Wang C, Matthan NR, Klett EL *et al.* (2018) A role for long-chain acyl-CoA synthetase-4 (ACSL4) in diet-induced phospholipid remodeling and obesity-associated adipocyte dysfunction. *Mol Metab* **9**, 43–56.
- 39 Ubellacker JM, Tasdogan A, Ramesh V, Shen B, Mitchell EC, Martin-Sandoval MS, Gu Z, McCormick ML, Durham AB, Spitz DR *et al.* (2020) Lymph protects metastasizing melanoma cells from ferroptosis. *Nature* **585**, 113–118.
- 40 Padanad MS, Konstantinidou G, Venkateswaran N, Melegari M, Rindhe S, Mitsche M, Yang C, Batten K, Huffman KE, Liu J *et al.* (2016) Fatty acid oxidation mediated by acyl-CoA synthetase long chain 3 is required for mutant KRAS lung tumorigenesis. *Cell Rep* **16**, 1614–1628.
- 41 Sen N, Gui B and Kumar R (2014) Physiological functions of MTA family of proteins. *Cancer Metastasis Rev* **33**, 869–877.
- 42 Zhang H, Stephens LC and Kumar R (2006) Metastasis tumor antigen family proteins during breast cancer progression and metastasis in a reliable mouse model for human breast cancer. *Clin Cancer Res* **12**, 1479–1486.
- 43 Monzon FA, Alvarez K, Peterson L, Truong L, Amato RJ, Hernandez-McClain J, Tannir N, Parwani AV and Jonasch E (2011) Chromosome 14q loss defines a molecular subtype of clear-cell renal cell carcinoma associated with poor prognosis. *Mod Pathol* **24**, 1470–1479.
- 44 Hsieh JJ, Le VH, Oyama T, Ricketts CJ, Ho TH and Cheng EH (2018) Chromosome 3p loss-orchestrated VHL, HIF, and epigenetic deregulation in clear cell renal cell carcinoma. *J Clin Oncol* **36**, 3533–3539.
- 45 Jonasch E, Walker CL and Rathmell WK (2021) Clear cell renal cell carcinoma ontogeny and mechanisms of lethality. *Nat Rev Nephrol* **17**, 245–261.
- 46 Gossage L and Eisen T (2010) Alterations in VHL as potential biomarkers in renal cell carcinoma. *Nat Rev Clin Oncol* **7**, 277–288.
- 47 Kaelin WG Jr (2008) The von Hippel-Lindau tumor suppressor protein: O₂ sensing and cancer. *Nat Rev Cancer* **8**, 865–873.
- 48 Weinberg RA (2014) *The Biology of Cancer*. 2nd edn. Garland Science Press, Garland Science, NY.
- 49 Gross DJ, Reibstein I, Weiss L, Slavin S, Dafni H, Neeman M, Pines M and Nagler A (2003) Treatment with halofuginone results in marked growth inhibition of a von Hippel-Lindau pheochromocytoma in vivo. *Clin Cancer Res* **9**, 3788–3793.
- 50 George DJ (2007) Phase 2 studies of sunitinib and AG013736 in patients with cytokine-refractory renal cell carcinoma. *Clin Cancer Res* **13**, 753–757.

- 51 Clark PE (2009) The role of VHL in clear-cell renal cell carcinoma and its relation to targeted therapy. *Kidney Int* **76**, 939–945.
- 52 Hiles JJ and Kolesar JM (2008) Role of sunitinib and sorafenib in the treatment of metastatic renal cell carcinoma. *Am J Health Syst Pharm* **65**, 123–131.
- 53 Powles T, Atkins MB, Escudier B, Motzer RJ, Rini BI, Fong L, Joseph RW, Pal SK, Sznol M, Hainsworth J *et al.* (2021) Efficacy and safety of atezolizumab plus bevacizumab following disease progression on atezolizumab or sunitinib monotherapy in patients with metastatic renal cell carcinoma in IMmotion150: a randomized phase 2 clinical trial. *Eur Urol* **79**, 665–673.
- 54 Wehn PM, Rizzi JP, Dixon DD, Grina JA, Schlachter ST, Wang B, Xu R, Yang H, Du X, Han G *et al.* (2018) Design and activity of specific hypoxia-inducible factor-2 α (HIF-2 α) inhibitors for the treatment of clear cell renal cell carcinoma: discovery of clinical candidate (S)-3-((2,2-Difluoro-1-hydroxy-7-(methylsulfonyl)-2,3-dihydro-1 H-inden-4-yl)oxy)-5-fluorobenzonitrile (PT2385). *J Med Chem* **61**, 9691–9721.
- 55 Xu R, Wang K, Rizzi JP, Huang H, Grina JA, Schlachter ST, Wang B, Wehn PM, Yang H, Dixon DD *et al.* (2019) 3-[(1S,2S,3R)-2,3-Difluoro-1-hydroxy-7-methylsulfonylindan-4-yl]oxy-5-fluorobenzonitrile (PT2977), a hypoxia-inducible factor 2 α (HIF-2 α) inhibitor for the treatment of clear cell renal cell carcinoma. *J Med Chem* **62**, 6876–6893.
- 56 Wallace EM, Rizzi JP, Han G, Wehn PM, Cao Z, Du X, Cheng T, Czerwinski RM, Dixon DD, Goggin BS *et al.* (2016) A small-molecule antagonist of HIF2 α is efficacious in preclinical models of renal cell carcinoma. *Cancer Res* **76**, 5491–5500.
- 57 Chen W, Hill H, Christie A, Kim MS, Holloman E, Pavia-Jimenez A, Homayoun F, Ma Y, Patel N, Yell P *et al.* (2016) Targeting renal cell carcinoma with a HIF-2 antagonist. *Nature* **539**, 112–117.
- 58 Liu Y, Fan J, Yan Y, Dang X, Zhao R, Xu Y and Ding Z (2020) JMY expression by Sertoli cells contributes to mediating spermatogenesis in mice. *FEBS J* **287**, 5478–5497.

Supporting information

Additional supporting information may be found online in the Supporting Information section at the end of the article.

Table S1. Primer sequences for qPCR.

Fig. S1. Effects of *RNASET2* knockdown or overexpression on ccRCC cells. (A) *RNASET2* knockdown in 786-O cells had no significant effect on the expression of lipolysis-related genes, $n = 6$; (B) Viability of 786-O cells was evaluated with the CCK-8 kit. The results showed that *RNASET2* shRNA transfection suppressed this parameter, $n = 4$; (C) *RNASET2* knockdown downregulated metastasis-associated genes MTA2 in 786-O cells, $n = 6$; (D) *RNASET2* overexpression in 769-P cells upregulated the expressions of DGAT1 and DGAT2 but did not influence RIP140 expression, $n = 6$; (E) *RNASET2* overexpression in 769-P cells did not influence cell proliferation. Values in bar graphs are the mean with SD. Statistical analysis was performed using the Student's *t*-test. * $P < 0.05$, ** $P < 0.01$, **** $P < 0.0001$; ns, not significant.

Fig. S2. Protein levels in ccRCC tissues and ANT. (A) Western blot analysis showed that the HIF1 α protein was deficient in ccRCC tissues; (B) Western blot analysis showed that the HIF2 α protein expression level was higher in ccRCC tissues than that in ANT.

Fig. S3. Results of coimmunoprecipitation and MS: *RNASET2* antibody pulled down proteins in 786-O cells. KEGG pathway analysis, the arrow points to metabolic pathways.